

# Laser-driven semiconductor switch for generating nanosecond pulses from a megawatt gyrotron

Cite as: Appl. Phys. Lett. **114**, 164102 (2019); doi: [10.1063/1.5093639](https://doi.org/10.1063/1.5093639)

Submitted: 22 February 2019 · Accepted: 4 April 2019 ·

Published Online: 24 April 2019






View Online



Export Citation



CrossMark

Julian F. Picard,<sup>a)</sup>  Samuel C. Schaub,  Guy Rosenzweig,  Jacob C. Stephens,  Michael A. Shapiro,   
and Richard J. Temkin 

## AFFILIATIONS

Plasma Science and Fusion Center, Massachusetts Institute of Technology, Cambridge, Massachusetts 02139, USA

<sup>a)</sup>Electronic mail: [jpicard@mit.edu](mailto:jpicard@mit.edu)

## ABSTRACT

A laser-driven semiconductor switch (LDSS) employing silicon (Si) and gallium arsenide (GaAs) wafers has been used to produce nanosecond-scale pulses from a 3  $\mu$ s, 110 GHz gyrotron at the megawatt power level. Photoconductivity was induced in the wafers using a 532 nm laser, which produced 6 ns, 230 mJ pulses. Irradiation of a single Si wafer by the laser produced 110 GHz RF pulses with a 9 ns width and >70% reflectance. Under the same conditions, a single GaAs wafer yielded 24 ns 110 GHz RF pulses with >78% reflectance. For both semiconductor materials, a higher value of reflectance was observed with increasing 110 GHz beam intensity. Using two active wafers, pulses of variable length down to 3 ns duration were created. The switch was tested at incident 110 GHz RF power levels up to 600 kW. A 1-D model is presented that agrees well with the experimentally observed temporal pulse shapes obtained with a single Si wafer. The LDSS has many potential uses in high power millimeter-wave research, including testing of high-gradient accelerator structures.

Published under license by AIP Publishing. <https://doi.org/10.1063/1.5093639>

Laser-driven semiconductor switches (LDSSs) are of great use in producing short RF pulses in the microwave to far-infrared range.<sup>1–5</sup> An LDSS-based system, like the experiment presented in this paper, operates by using a laser to induce temporary reflectance in a semiconductor wafer. The wafer subsequently reflects RF from a source for a short time period ranging from picoseconds to seconds. Semiconductors used in LDSS, such as silicon (Si) or gallium arsenide (GaAs), are dielectric materials with very low RF loss. When laser radiation is applied at a frequency such that the photon energy is greater than the semiconductor bandgap energy, an additional free-carrier population,  $n_c$ , is generated. This population can be simply treated as an electron-hole plasma. When  $n_c$  increases enough to raise the plasma frequency above the operational frequency of the RF source, the semiconductor becomes reflecting to the incident microwaves. The duration of the reflected pulse depends upon the intensity and width of the excitation laser pulse as well as the recombination time of the electron-hole plasma within the semiconductor.<sup>1</sup>

The fundamental behavior of LDSS systems in generating short pulses has been well characterized by previous experiments at lower RF power levels.<sup>3,4,6–11</sup> Theoretical work investigating the semiconductor response has been completed for both fundamental waveguide and free-space systems.<sup>3,12,13</sup> LDSS systems have been applied to electron spin resonance spectroscopy, notably in 2014 using a 150 W gyrotron

at 154 GHz as the RF source.<sup>5</sup> At the kilowatt power level, LDSS modulators have been tested with a pulsed subterahertz gyrotron at IAP, Russia,<sup>14</sup> lasers at the Institute for Terahertz Science and Technology at the University of California, Santa Barbara<sup>15,16</sup> and the Institute of Scientific and Industrial Research at Osaka University.<sup>17</sup>

The experiment discussed in this paper extends the previous work by demonstrating LDSS operation with a megawatt power level, 110 GHz gyrotron. We characterize the response of Si and GaAs reflectance as a function of both incident laser energy and incident 110 GHz RF intensity. The pulses created have widths on the nanosecond timescale and power levels of hundreds of kilowatts.

The experimental setup is shown in Fig. 1. A megawatt gyrotron is used as the input power source. The gyrotron produces a 3  $\mu$ s pulse with flat-top power up to 1.5 MW at 110 GHz.<sup>18</sup> The gyrotron output couples to the  $HE_{11}$  mode of a 31.75 mm diameter corrugated waveguide.<sup>19</sup> Power from the gyrotron is modulated using a continuously variable quasi-optical microwave attenuator, consisting of five quartz plates at the Brewster angle and a sapphire half-waveplate. The output of this attenuator feeds the input waveguide on the right in Fig. 1. Small reflections into the gyrotron from the experimental setup limited the maximum input power to the LDSS experiment to 600 kW.

The experiment was designed for both single- and dual-wafer operation. In single-wafer operation, only the primary wafer is

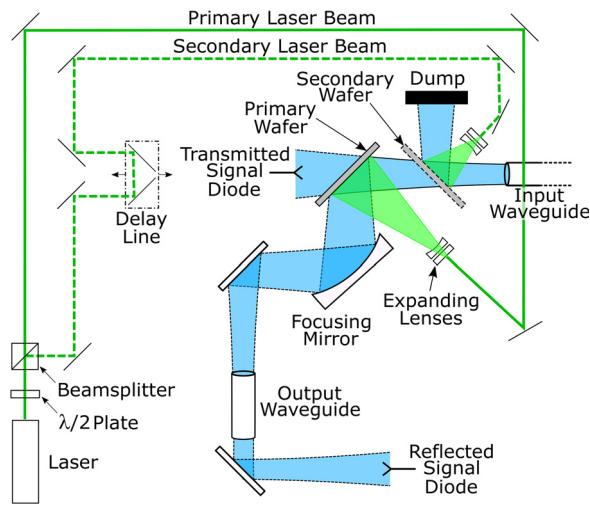


**FIG. 1.** Experimental setup of the LDSS experiment. 110 GHz microwaves, seen in blue, are generated by the MIT megawatt gyrotron (not shown) and enter the setup from the input waveguide. Primary and secondary laser beams are shown in green.

installed and the primary laser beam is active. A  $3\ \mu\text{s}$  RF pulse from the gyrotron is incident upon the primary wafer, which is initially transparent at 110 GHz. With no incident laser light, the GaAs and Si wafers absorb  $<0.1\%$  of the incident RF power. The primary wafer becomes reflective when illuminated by the primary laser beam and redirects the microwaves towards the output stage (discussed below). Reflection continues until the charge carrier density in the wafer decays back to below the cutoff density,  $n_c$ , and the wafer again becomes transparent. The cutoff density is defined as  $n_c = (\omega_{RF}^2 m_e \epsilon_0) / e^2$ , where  $\omega_{RF}$  is the frequency of incident microwaves,  $\epsilon_0$  is the vacuum permittivity,  $m_e$  is the electron mass, and  $e$  is the fundamental charge. The output pulse width is determined by the parameters of the laser pulse (duration, intensity), as well as by the charge recombination rate of the primary wafer. In dual-wafer operation, the secondary wafer is also installed. At a time  $\Delta t$  after the primary wafer is illuminated, the secondary wafer is illuminated by the secondary laser beam. The excitation of the secondary wafer redirects the input RF to a beam dump, truncating the output to a pulse width of  $\Delta t$ . Adjusting an optical delay line varies  $\Delta t$ .

Photoconductivity in the semiconductor is induced using a Quantel Q-smart 450 laser with a frequency doubling stage. The Q-switched Nd:YAG laser produces an  $\sim 6\ \text{ns}$  FWHM pulse at 532 nm with a beam diameter of 6.5 mm. The maximum energy per pulse is 230 mJ. This wavelength was chosen to ensure that the excitation photon energy (2.33 eV) is sufficiently above the bandgap of Si (1.11 eV) and GaAs (1.43 eV). The combination of a half-waveplate and polarizing beamsplitter at the output of the laser allows the distribution of energy between the primary and secondary laser beams to be varied.

The transmitted signal diode is used to quantify the input power, as shown in Fig. 1. After being reflected from the wafer, a custom elliptical mirror refocuses the microwave beam, coupling to the  $\text{HE}_{11}$  mode of the output waveguide. After the waveguide, the RF pulse is sampled by the reflected signal diode, as seen at the bottom of Fig. 1. The Schottky diode detectors were calibrated *in situ* with a calorimeter.

Both Si and GaAs wafers were tested. The 100 mm diameter wafers were purchased from University Wafer (U.W.) with custom

thicknesses ( $407\ \mu\text{m}$  for GaAs and  $387\ \mu\text{m}$  for Si) specified to prevent reflection of the linearly polarized 110 GHz gyrotron pulse during the quiescent state in accordance with the etalon effect at a  $45^\circ$  incident angle.

Figure 2(a) shows a characteristic laser pulse (averaged over 100 pulses) with a total energy of 215 mJ. The peak laser intensity on the wafer is  $3.5\ \text{MW}/\text{cm}^2$ , and the total energy density is  $15.3\ \text{mJ}/\text{cm}^2$ . The structure of the 6 ns pulse is caused by the multilongitudinal modes of the laser cavity. The laser illuminates the wafer at normal incidence and is close to uniform over the elliptical active region with a minor radius of 1.8 cm and a major radius of 2.5 cm.

Characteristic 110 GHz reflected pulses (averaged over 10 pulses) from the different wafers are featured in Fig. 2(b). The incident 525 kW, 110 GHz gyrotron pulse (not shown) had a duration of  $3\ \mu\text{s}$ . The beam has a Gaussian spatial distribution with a 1.7 cm waist at the primary wafer, which is illuminated at a  $45^\circ$  angle. The laser pulse energy was 215 mJ. Under these conditions, the Si wafer produced a reflected 110 GHz RF pulse with a 9 ns width. The peak reflected power is 410 kW, corresponding to 78% of the input power. Under the same conditions, the GaAs wafer yielded a 24 ns reflected pulse. With a peak reflected power of 485 kW, the GaAs wafer reflects 92% of the input RF power. The reflectance persists near its maximum level for  $\sim 10\ \text{ns}$  after peak laser intensity and then decays to negligible levels within 30 ns. The dual-wafer pulse was generated using Si as the primary wafer and GaAs as the secondary wafer due to the latter's longer observed recombination time. The dual-wafer pulse has a width of 3 ns and a peak RF power of 300 kW. The pulse width can be continuously varied by adjusting the optical delay line.

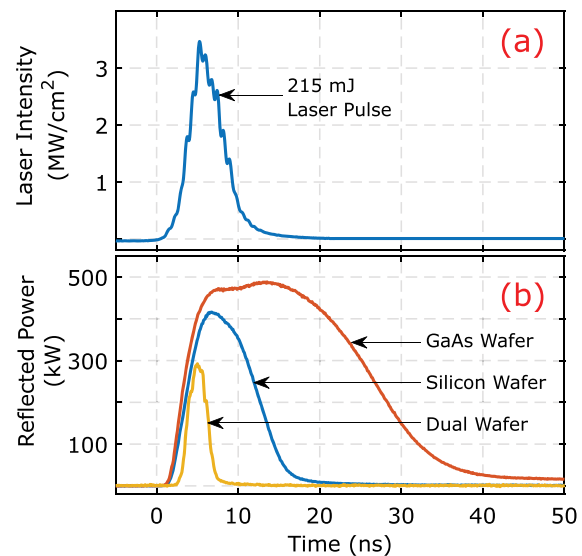


**FIG. 2.** (a) Experimentally measured temporal profile of the 532 nm laser pulse used to excite the Si and GaAs wafers. The modal structure is inherent to the laser design. (b) Characteristic reflected pulses from the GaAs wafer (red) and the Si wafer (blue) in single-wafer operation, with 525 kW of incident 110 GHz RF power and 215 mJ of incident laser energy. Dual-wafer operation is in yellow, with Si as the primary wafer (illuminated by 120 mJ of laser energy) and GaAs as the secondary wafer (illuminated by 100 mJ of laser energy). Adjusting the optical delay line (see Fig. 1) allows for continuous variation of the dual-wafer pulse width.

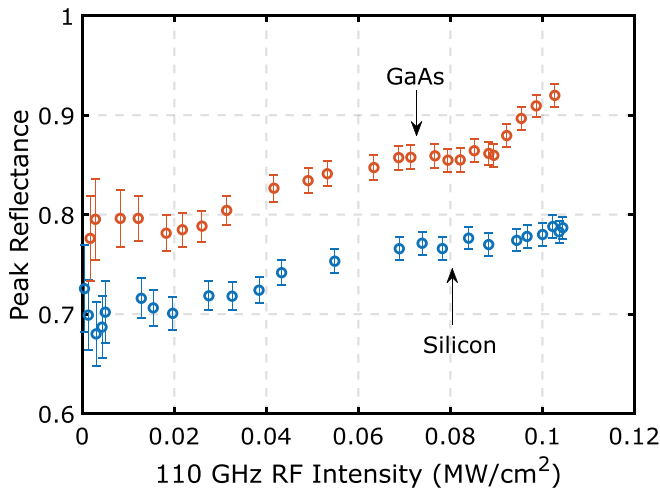
Experiments were conducted to measure the reflectance of the Si and GaAs wafers as a function of incident 110 GHz RF intensity. The results can be seen in Fig. 3, which demonstrates that at high incident microwave power, the peak reflectance of both Si and GaAs wafers increases. These data were collected at the maximum available laser energy density of  $15.3 \text{ mJ/cm}^2$ . At low RF intensity, GaAs has a reflectance of  $78\% \pm 1\%$ , which increases to  $92\% \pm 1\%$  at a maximum RF intensity of  $0.104 \text{ MW/cm}^2$ , corresponding to 525 kW total incident power. Similarly, the Si wafer has a low-intensity reflectance of  $70\% \pm 1\%$ , increasing to  $78\% \pm 1\%$  at high RF power. Despite the enhancement in peak reflectance, there was no observed change in the overall shape of the reflected pulses from either Si or GaAs over the range of 25–525 kW of 110 GHz RF power.

Figure 4 demonstrates the dependence of Si and GaAs wafer reflectance on laser energy density. Reflectance tends towards zero with no laser energy, as expected. The characteristic shape of the curves exhibits a “saturation” behavior that has been observed extensively in previous experiments.<sup>3,15,20</sup> While the GaAs curve appears to reach saturation around  $8 \text{ mJ/cm}^2$ , the Si wafer does not reach complete saturation even at the maximum energy density. This might indicate that additional laser energy would allow for a more thorough characterization of the Si wafer behavior. In Fig. 4, the maximum laser energy density of  $15.3 \text{ mJ/cm}^2$  corresponds to 215 mJ of total laser energy.

To explain the recombination times observed, the photoconductivity effects of the Si wafer were numerically simulated using the same physical model employed by Vogel *et al.*<sup>13</sup> The model is a 1-D reaction-diffusion model, where the equation governing carrier density,  $n_c$ , is

$$\frac{\partial n_c(z, t)}{\partial t} = \frac{\eta\alpha}{h\nu A_l} P_l(t) e^{-\alpha z} + D \frac{\partial^2 n_c(z, t)}{\partial z^2} - \gamma_1 n_c(z, t) - \gamma_2 n_c^2(z, t) - \gamma_3 n_c^3(z, t). \quad (1)$$

The first term on the right hand side of Eq. (1) accounts for the generation of electron-hole pairs by laser illumination over an area  $A_l$ ,



**FIG. 3.** Peak reflectance vs 110 GHz RF intensity. The maximum RF intensity of  $0.104 \text{ MW/cm}^2$  corresponds to 525 kW of total incident power. All data was taken at a laser energy density of  $15.3 \text{ mJ/cm}^2$  (215 mJ of total laser energy).

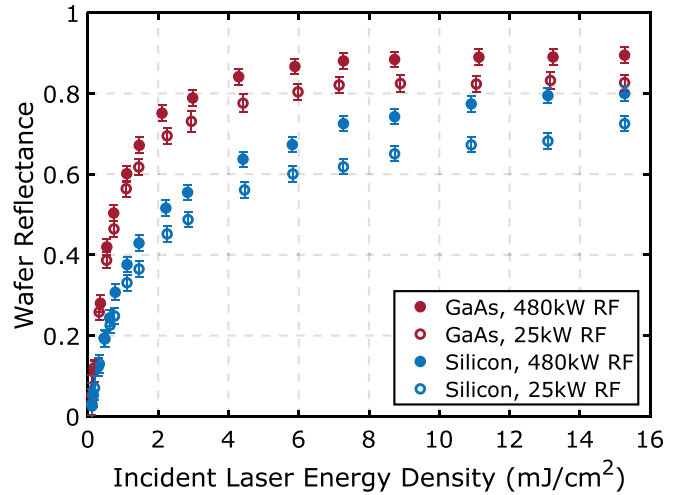


**FIG. 4.** Peak reflectance vs laser energy density for GaAs and Si wafers at low (25 kW) and high (480 kW) incident 110 GHz RF power. The maximum laser energy density of  $15.3 \text{ mJ/cm}^2$  corresponds to 215 mJ of total incident laser energy.

for a laser power  $P_l(t)$  that is taken to be a Gaussian pulse in time with a 7 ns width. The photon energy is  $h\nu$ . The factor of  $\eta$ , taken to be 0.35, accounts for both reflection of light from the substrate (measured to be  $\sim 65\%$ ) and quantum efficiency (assumed to be 1).<sup>13</sup> The laser intensity exponentially decays in the wafer, with an attenuation constant  $\alpha = 10^6 \text{ m}^{-1}$ . The diffusion constant,  $D$ , is taken to be  $17.9 \text{ cm}^2 \text{ s}^{-1}$  for Si. The last three terms represent bulk recombination. The radiative ( $\gamma_2$ ) and Auger ( $\gamma_3$ ) recombination rates are well known, with  $\gamma_2 = 3.3 \times 10^{-21} \text{ m}^3 \text{ s}^{-1}$  and  $\gamma_3 = 3.8 \times 10^{-43} \text{ m}^6 \text{ s}^{-1}$ . The impurity recombination rate ( $\gamma_1$ ) is strongly dependent on the quality and composition of the silicon and is taken to be the first free parameter in the model.

A damped Drude representation of the permittivity is utilized for the electron-hole plasma

$$\varepsilon = \varepsilon_L - \frac{\omega_{p,e}^2}{\omega(\omega + i/\tau_{D,e})} - \frac{\omega_{p,h}^2}{\omega(\omega + i/\tau_{D,h})}. \quad (2)$$

The unexcited permittivity of Si,  $\varepsilon_L$ , is taken to be 11.68. The electron and hole plasma frequencies are  $\omega_{p,(e,h)}^2 = n_{e,h}e^2/m_{e,h}^*\varepsilon_0$ , where  $e$  is the elementary charge and  $\varepsilon_0$  is the vacuum permittivity. The effective optical masses of electrons and holes are taken to be  $m_e^* = 0.2588m_e$  and  $m_h^* = 0.2063m_e$ , respectively, where  $m_e$  is the electron rest mass.  $\tau_{D,(e,h)}$  are the Drude damping times. Since the impurity content of our wafers is unknown, we use these damping times as the second and third fitting parameters.

Figure 5 compares the results of the numerical simulation with a characteristic reflected pulse from the Si wafer at low RF power, showing very good agreement. Figure 6 also shows very good agreement between the model and the response of the Si wafer to varying laser energy densities. The fit to experimental data was generated with the parameter values  $\gamma_1 = 3 \times 10^8 \text{ s}^{-1}$ ,  $\tau_{D,e} = 0.199 \text{ ps}$ , and  $\tau_{D,h} = 0.056 \text{ ps}$ .

In pulses produced by either wafer material, the rise time of the reflected pulse is dominated by the rise time of the laser pulse. This is

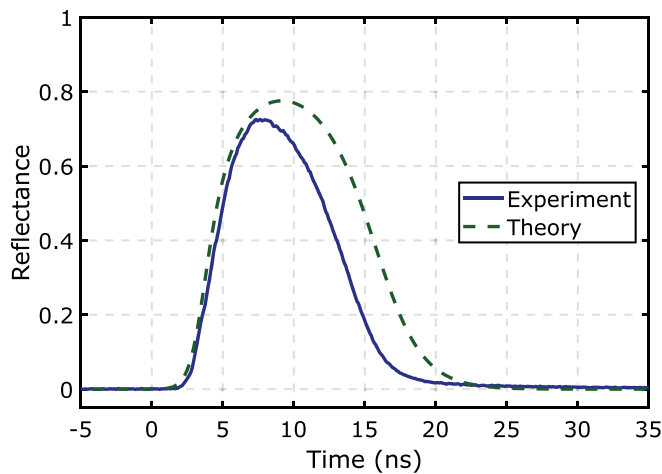


**FIG. 5.** Comparison of experiment and numerical simulation for a characteristic pulse reflected from the excited Si wafer at low RF power. Fitting parameters of  $\gamma_1 = 3 \times 10^8 \text{ s}^{-1}$ ,  $\tau_{D,e} = 0.199 \text{ ps}$ , and  $\tau_{D,h} = 0.056 \text{ ps}$  show very good agreement with the experimental results.

consistent with previous experiments that demonstrated subnanosecond risetimes using a similar setup but faster laser pulses.<sup>15–17</sup> The fall time of the reflected pulse is dictated by the duration and intensity of the laser pulse as well as the recombination time of the semiconductor. The recombination time of the GaAs wafer is approximately 30 ns and is comparable to values seen in previous experiments that used a laser pulse of a similar duration.<sup>3,4</sup>

The reflected power from the Si wafer begins to decay almost immediately after the laser pulse reaches its peak intensity, resulting in a fall time on the order of 10 ns for the Si reflected pulses. This is much shorter than was found in most previous experiments, which observed recombination times that range from hundreds of nanoseconds to milliseconds in undoped high-resistivity Si wafers.<sup>3,6,13,16,21</sup>

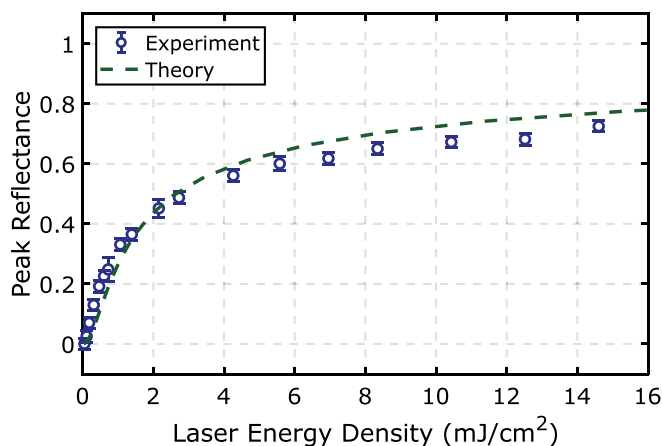


**FIG. 6.** Comparison of experiment and numerical simulation for the relationship between the laser energy density and peak reflectance for the Si wafer at low RF power.

Near the peak of the simulated reflected pulse (Fig. 5, dashed), impurity ( $\gamma_1 n_c$ ) and Auger ( $\gamma_3 n_c^3$ ) rates are comparable, and both play a substantial role in recombination. Below  $R \approx 0.4$ , impurity recombination strongly dominates, driving the rapid decrease in reflectance to zero.

Because the recombination time observed in the silicon wafers acquired from U.W. was very short, we tested a set of silicon wafers from a second vendor, Nova Electronic Materials. These wafers produced pulses with a duration of several microseconds, which is consistent with the results previously obtained in other studies. This suggests that the very short pulse width of the U.W. wafers is an intrinsic property of those samples.

We then attempted to determine the properties of the U.W. wafers responsible for the short pulse duration. Our measurements of resistivity verified that wafers from both U.W. and Nova Electronic Materials meet the high ( $>5000 \Omega \text{ cm}$ ) resistivity specification provided during purchase. Although both sets of wafers were specified as undoped, we also investigated the impurity content. One prior experiment showed a 10 ns recombination time using a Si wafer that was doped with gold.<sup>21</sup> The wafers acquired from U.W. were submitted for analysis by both Glow Discharge Mass Spectrometry and Secondary Ion Mass Spectrometry. Only low levels of trace impurities were found: Boron at  $\leq 10 \text{ ppb}$  by weight and Phosphorus at  $\leq 20 \text{ ppb}$  by weight. As a result, we do not have a clear explanation for the nanosecond pulse decay times observed using the U.W. wafers at this time.

In summary, this work has demonstrated operation of an LDSS-based millimeter-wave modulator in the creation of nanosecond-duration, megawatt-level pulses at 110 GHz. At low 110 GHz RF power, reflectance values for the Si and GaAs wafers are comparable to the values measured in previous experiments.<sup>15,16</sup> With 525 kW of incident RF power, the reflectances of both Si and GaAs wafers were seen to increase by approximately 10%. Some absorption of incident RF by the wafer takes place during photoconductivity and may be responsible for the observed increase in reflectivity with input RF power. The short pulses reflected from a Si wafer were accurately modeled using a numerical simulation based on the work by Vogel *et al.*<sup>13</sup> An important feature of the laser-driven semiconductor switch is the ability to generate extremely short pulses of variable width, down to 3 ns for a 300 kW pulse, which have been put to exciting use in testing a high-frequency, high-gradient accelerator concept developed at SLAC.<sup>22,23</sup>

The authors would like to thank the reviewers for their very helpful comments. This work was supported by the Department of Energy, Office of High Energy Physics under Grant No. DE-SC0015566, the Office of Fusion Energy Sciences through Grant No. DE-FC02-93ER54186, and the National Institutes of Health, National Institute for Biomedical Imaging and Bioengineering under Grant Nos. EB004866 and EB001965.

## REFERENCES

- <sup>1</sup>M. Rahm, J. Li, and W. J. Padilla, *J. Infrared, Millimeter, Terahertz Waves* **34**, 1 (2013).
- <sup>2</sup>A. Woldegeorgis, T. Kurihara, B. Beleites, J. Bossert, R. Grosse, G. G. Paulus, F. Ronneberger, and A. Gopal, *J. Infrared, Millimeter, Terahertz Waves* **39**, 667 (2018).
- <sup>3</sup>T. Nozokido, H. Minamide, and K. Mizuno, *Electron. Commun. Jpn.* **80**, 1 (1997).

- <sup>4</sup>M. L. Kulygin, V. I. Belousov, G. G. Denisov, A. A. Vikharev, V. V. Korchagin, A. V. Kuzin, E. A. Novikov, and M. A. Khozin, *Radiophys. Quantum Electron.* **57**, 509 (2014).
- <sup>5</sup>S. Mitsudo, C. Umegaki, Y. Fujii, and Y. Tatematsu, in *Proceedings of the IEEE 40th International Conference on Infrared Millimeter, Terahertz Waves, Hong Kong, China* (2015), p. 1.
- <sup>6</sup>M. S. Choe, A. Sawant, K.-S. Lee, N. E. Yu, and E. Choi, *Appl. Phys. Lett.* **110**, 074101 (2017).
- <sup>7</sup>D. H. Auston, *Appl. Phys. Lett.* **26**, 101 (1975).
- <sup>8</sup>G. Mourou, C. V. Stancampiano, A. Antonetti, and A. Orszag, *Appl. Phys. Lett.* **39**, 295 (1981).
- <sup>9</sup>C. H. Lee, *Appl. Phys. Lett.* **30**, 84 (1977).
- <sup>10</sup>M. L. Kulygin, G. G. Denisov, E. A. Novikov, A. P. Fokin, and I. A. Litovsky, *Radiophys. Quantum Electron.* **61**, 603 (2019).
- <sup>11</sup>M. Kulygin, G. Denisov, S. Shubin, S. Salahetdinov, and E. Novikov, *IEEE Trans. Terahertz Sci. Technol.* **7**, 225 (2017).
- <sup>12</sup>M. L. Kulygin, G. G. Denisov, and V. V. Kocharovskiy, *J. Infrared, Millimeter, Terahertz Waves* **31**, 31 (2010).
- <sup>13</sup>T. Vogel, G. Dodel, E. Holzhauer, H. Salzmänn, and A. Theurer, *Appl. Opt.* **31**, 329 (1992).
- <sup>14</sup>M. Kulygin, *IEEE Trans. Terahertz Sci. Technol.* **9**, 186 (2019).
- <sup>15</sup>S. Takahashi, L. Brunel, D. T. Edwards, J. van Tol, G. Ramian, S. Han, and M. S. Sherwin, *Nature* **489**, 409 (2012).
- <sup>16</sup>F. A. Hegmann and M. S. Sherwin, in *Proceedings of the SPIE 2842, Millimeter and Submillimeter Waves and Applications III* (1996), p. 90.
- <sup>17</sup>K. Kawase, R. Kato, A. Irizawa, M. Fujimoto, K. Furukawa, K. Kubo, and G. Isoyama, in *Proceedings of the 37th International Free Electron Laser Conference (FEL 2015), Daejeon, Korea* (2015), p. 430.
- <sup>18</sup>E. M. Choi, C. D. Marchewka, I. Mastovsky, J. R. Sirigiri, M. A. Shapiro, and R. J. Temkin, *Phys. Plasmas* **13**, 023103 (2006).
- <sup>19</sup>J. M. Neilson, R. L. Ives, S. C. Schaub, W. C. Guss, G. Rosenzweig, R. J. Temkin, and P. M. Borchard, *IEEE Trans. Electron Devices* **65**, 2316 (2018).
- <sup>20</sup>M. Kulygin, G. Denisov, K. Vlasova, N. Andreev, S. Shubin, and S. Salahetdinov, *Rev. Sci. Instrum.* **87**, 014704 (2016).
- <sup>21</sup>A. A. Vikharev, G. G. Denisov, V. V. Kocharovskiy, S. V. Kuzikov, V. V. Parshin, N. Y. Peskov, A. N. Stepanov, D. I. Sobolev, and M. Y. Shmelev, *Tech. Phys. Lett.* **33**, 735–737 (2007).
- <sup>22</sup>E. Nanni, V. Dolgashev, A. Haase, S. Jawla, J. Neilson, S. Schaub, B. Spataro, S. Tantawi, and R. Temkin, in *Proceedings of the 9th International Particle Accelerator Conference (IPAC'18), Vancouver, BC, Canada* (2018), p. TUZGBE4.
- <sup>23</sup>E. A. Nanni, V. Dolgashev, S. Jawla, J. Neilson, M. Othman, J. Picard, S. Schaub, B. Spataro, S. Tantawi, and R. J. Temkin, in *Proceedings of the IEEE 43th International Conference on Infrared Millimeter, Terahertz Waves, Nagoya, Japan* (2018), p. 1.